JOURNAL OF MOLECULAR SIGNALING

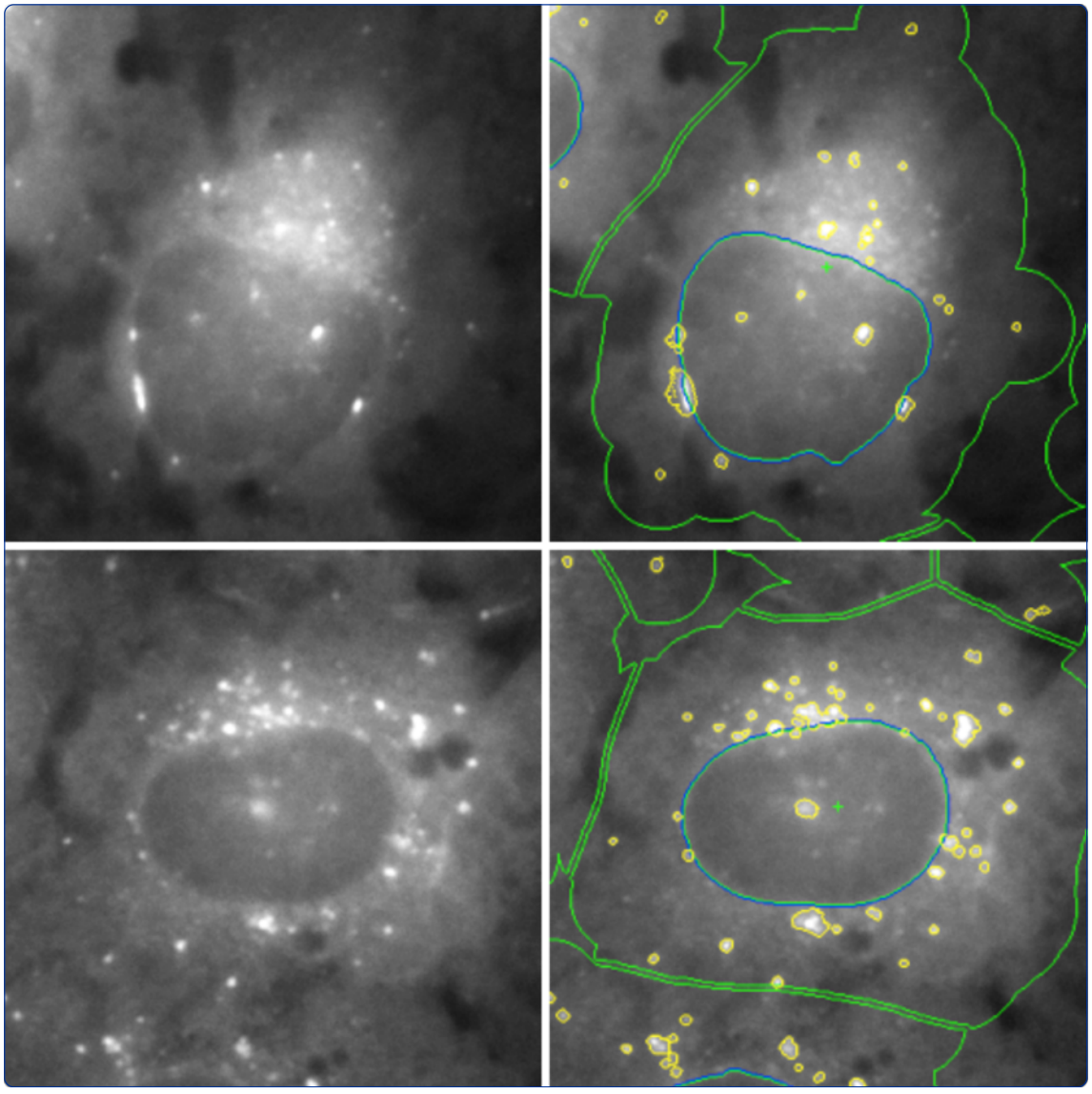

Defining regulatory and phosphoinositide-binding sites in the human WIPI-1 β-propeller responsible for autophagosomal membrane localization downstream of mTORC1 inhibition

Gaugel *et al.*

BioMed Central

Gaugel *et al. Journal of Molecular Signaling* 2012, **7**:16
http://www.jmolecularsignaling.com/content/7/1/16

JOURNAL OF MOLECULAR SIGNALING

RESEARCH ARTICLE Open Access

Defining regulatory and phosphoinositide-binding sites in the human WIPI-1 β-propeller responsible for autophagosomal membrane localization downstream of mTORC1 inhibition

Anja Gaugel, Daniela Bakula, Anneliese Hoffmann and Tassula Proikas-Cezanne*

Abstract

Background: Autophagy is a cytoprotective, lysosomal degradation system regulated upon induced phosphatidylinositol 3-phosphate (PtdIns(3)P) generation by phosphatidylinositol 3-kinase class III (PtdIns3KC3) downstream of mTORC1 inhibition. The human PtdIns(3)P-binding β-propeller protein WIPI-1 accumulates at the initiation site for autophagosome formation (phagophore), functions upstream of the Atg12 and LC3 conjugation systems, and localizes at both the inner and outer membrane of generated autophagosomes. In addition, to a minor degree WIPI-1 also binds PtdIns(3,5)P_2. By homology modelling we earlier identified 24 evolutionarily highly conserved amino acids that cluster at two opposite sites of the open Velcro arranged WIPI-1 β-propeller.

Results: By alanine scanning mutagenesis of 24 conserved residues in human WIPI-1 we define the PtdIns-binding site of human WIPI-1 to critically include S203, S205, G208, T209, R212, R226, R227, G228, S251, T255, H257. These amino acids confer PtdIns(3)P or PtdIns(3,5)P_2 binding. In general, WIPI-1 mutants unable to bind PtdIns(3)P/PtdIns(3,5)P_2 lost their potential to localize at autophagosomal membranes, but WIPI-1 mutants that retained PtdIns(3)P/PtdIns(3,5)P_2 binding localized at Atg12-positive phagophores upon mTORC1 inhibition. Both, downregulation of mTOR by siRNA or cellular PtdIns(3)P elevation upon PIKfyve inhibition by YM201636 significantly increased the localization of WIPI-1 at autophagosomal membranes. Further, we identified regulatory amino acids that influence the membrane recruitment of WIPI-1. Exceptional, WIPI-1 R110A localization at Atg12-positive membranes was independent of autophagy stimulation and insensitive to wortmannin. R112A and H185A mutants were unable to bind PtdIns(3)P/PtdIns(3,5)P_2 but localized at autophagosomal membranes, although in a significant reduced number of cells when compared to wild-type WIPI-1.

Conclusions: We identified amino acids of the WIPI-1 β-propeller that confer PtdIns(3)P or PtdIns(3,5)P_2 binding (S203, S205, G208, T209, R212, R226, R227, G228, S251, T255, H257), and that regulate the localization at autophagosomal membranes (R110, R112, H185) downstream of mTORC1 inhibition.

Keywords: Autophagosome, Autophagy, Atg12, Atg18, Phagophore, PtdIns3KC3, PtdIns(3)P, PtdIns(3,5)P_2, WIPI-1, YM201636

* Correspondence: tassula.proikas-cezanne@uni-tuebingen.de
From the Autophagy Laboratory, Department of Molecular Biology, Interfaculty Institute of Cell Biology, Eberhard Karls University Tuebingen, Auf der Morgenstelle 15, 72076, Tuebingen, Germany

Background

Macroautophagy (hereafter referred to as autophagy) is defined as a stochastic lysosomal bulk degradation pathway for cytoplasmic material, and characterized by membrane rearrangements from autophagosome formation to fusion events with the lysosomal compartment. In addition, autophagy selectively targets the degradation of protein aggregates, damaged organelles and invading pathogens. Stochastic and selective autophagy control both turnover and clearance of the cytoplasm, thereby critically contributing to eukaryotic cell homeostasis (for review see e.g. [1-4]).

The autophagosomal membrane is of as yet uncertain origin [5], but recent reports provide evidence that multiple membrane systems, such as the endoplasmic reticulum [6,7] or the plasma membrane [8] contribute to autophagosome formation from initial template membranes (phagophore). Phagophores are proposed to elongate to double-membrane autophagosomes by receiving membrane input from the endocytic compartment, critically involving Atg9-positive vesicles [9]. Autophagosomes sequester the cytoplasmic cargo and communicate or fuse with the lysosomal compartment to permit final degradation [10].

The AMPK/mTORC1 sensing system for nutrient, energy and hormone level modulates the onset of autophagy via differential phosphorylation of the Ulk1-Atg13-FIP200 complex [11-15]. Within this control circuit, mTORC1 negatively regulates autophagy, first demonstrated by rapamycin-mediated induction of autophagy [16]. mTORC1 inhibition promotes the activation of phosphatidylinositol-3 kinase class III (PtdIns3KC3, Vps34) that generates phosphatidylinositol 3-phosphate (PtdIns(3)P) [17,18]. Generation of PtdIns(3)P is prerequisite for the formation of autophagosomes [19], first demonstrated by the employment wortmannin, an irreversible phosphatidylinositol 3-kinase inhibitor [20].

PtdIns3KC3 becomes engaged in the initiation of autophagy through complex formation with Beclin 1, p150 (Vps15) and Atg14L, the latter recruiting PtdIns3KC3 to the ER [21,22] where PtdIns(3)P-effectors subsequently contribute to the formation of autophagosomes [23-25]. PtdIns(3)P-binding proteins shown to be involved in the process of autophagy include Alfy [26] and DFCP1 [23,27] both of which bind PtdIns(3)P at phagophore precursors via their the FYVE-domain [28]. Factors belonging to the WD-repeat protein interacting with phosphoinositide (WIPI) family fold into seven-bladed β-propeller proteins with an open Velcro topology and bind PtdIns(3)P at the phagophore [29-31]. Human WIPI-1 and WIPI-2 evolved from the ancestral yeast Atg18 protein and share an essential function during autophagosome formation upstream of the Atg12 and LC3 conjugation systems, hence regulate LC3 conjugation to phosphatidylethanolamine (LC3-II) [24,29,32]. WIPI-1 localizes to both ER and PM, and WIPI-2 was found to localize close to the Golgi area and to the PM upon the induction of autophagy [33]. Further, both WIPI-1 and WIPI-2 were detected at the inner and outer autophagosomal membrane [33]. From this, WIPI-1 and WIPI-2 should function as PtdIns(3)P effectors essential for decoding the PtdIns(3)P signal downstream of PtdIns3KC3, thereby permitting the recruitment of downstream autophagy-related (Atg) proteins [34,35].

Our previous phylogenetic analyses identified 24 evolutionarily conserved amino acids specific to the 7-bladed WIPI beta-propeller protein family [29]. These conserved amino acids cluster at two proposed binding sites of the WIPI propeller: one less conserved across the top of propeller blades 1–3 and one highly conserved across the bottom of blades 4–7. We proposed that the conserved amino acid cluster across the bottom of blades 4–7 confers binding to phosphoinositides (PtdIns) [29], because two arginine residues (R226/R227) situated within were shown to be critical for PtdIns(3)P binding [36].

By alanine scanning mutagenesis of the 24 evolutionarily conserved amino acids of the WIPI family, we functionally define here the critical amino acids in human WIPI-1 responsible for PtdIns-binding and autophagosomal membrane recruitment upon the induction of autophagy.

Results

Site-directed alanine-screening mutagenesis of GFP-WIPI-1 (Table 1) was conducted to investigate the functional relationship of 24 conserved residues, unique to the WIPI protein family (Figure 1A, Additional file 1: Figure S1), with regard to both autophagosomal membrane localization (fluorescent puncta) and PtdIns-binding capabilities.

We initiated the characterization of the generated mutants by conducting quantitative, fluorescence-based GFP-WIPI-1 puncta-formation analysis [37,38] upon transient expression (48 h) of the GFP control, wild-type or either of the generated GFP-WIPI-1 mutant in human U2OS cells (Figure 1B) followed by the following 3 h treatments. Application of control medium (CM) was used to score for autophagosomal membrane localization of GFP-WIPI-1 in cells undergoing basal autophagy. Rapamycin (RM) was applied to inhibit mTORC1 hence to induce autophagy. Wortmannin (WM) was used to either inhibit basal autophagy, or in combination with rapamycin (RM/WM) to counteract the induction of autophagy. Rapamycin-mediated autophagy was controlled by LC3-lipidation assays (Additional file 2: Figure S2). The number of puncta-positive cells was quantified (n = 3) from 300 individual cells for each condition (Additional file 3:

Table 1 Site-directed mutagenesis of human WIPI-1

Mutant	Position	Mutation	PCR oligonucleotides (forward, reverse)
GFP-N23A	N67-68	AA to GC	AGCTGCTTCTCTTTCGCCCAGGACTGCACATCC,
			GGATGTGCAGTCCTGGGCGAAAGAGAAGCAGCT
GFP-Q24A	N70-71	CA to GC	CTCTTTCAACGCGGACTGCACATCCCTAGCAA,
			TTGCTAGGGATGTGCAGTCCGCGTTGAAAGAG
GFP-D25A	N74	A to C	TCTTTCAACCAGGCCTGCACATCCCTAGCA,
			TGCTAGGGATGTGCAGGCCTGGTTGAAAGA
GFP-E64A	N191	A to C	GTCTACATCGCGGCGCGCCTCTTCTCC,
			GGAGAAGAGGCGCGCCGCGATGTAGAC
GFP-R107A	N319-320	AG to GC	CAACATCTTGTCCATAGCGCTGAACCGGCAAAGGC,
			GCCTTTGCCGGTTCAGCGCTATGGACAAGATGTTG
GFP-R110A	N328-329	CG to GC	TCCATAAGGCTGAACGCGCAAAGGCTGCTGGTT,
			AACCAGCAGCCTTTGCGCGTTCAGCCTTATGGA
GFP-R112A	N334-335	AG to GC	GCTGAACCGGCAAGCGCTGCTGGTTTGCC,
			GGCAAACCAGCAGCGCTTGCCGGTTCAGC
GFP-H185A	N553-554	CA to GC	TGCACTATTGCTGCCGCTGAGGGAACACTAGCTGCC,
			GGCAGCTAGTGTTCCCTCAGCGGCAGCAATAGTGCA
GFP-G198A	N593	G to C	CACCTTCAATGCCTCAGCCTCCAAACTAGCA,
			TGCTAGTTTGGAGGCTGAGGCATTGAAGGTG
GFP-S203A	N607-608	AG to GC	GGCTCCAAACTAGCAGCTGCGTCTGAAAAAGGC,
			GCCTTTTTCAGACGCAGCTGCTAGTTTGGAGCC
GFP-S205A	N613	T to G	CTAGCAAGTGCGGCTGAAAAAGGCACAGTC,
			GACTGTGCCTTTTTCAGCCGCACTTGCTAG
GFP-G208A	N623	G to C	AGTGCGTCTGAAAAAGCCACAGTCATCCGG,
			CCGGATGACTGTGGCTTTTTCAGACGCACT
GFP-T209A	N625	A to G	TCTGAAAAAGGCGCAGTCATCCGGGTG,
			CACCCGGATGACTGCGCCTTTTTCAGA
GFP-R212A	N634-635	CG to GC	GGCACAGTCATCGCGGTGTTCTCTGTCCC,
			GGGACAGAGAACACCGCGATGACTGTGCC
GFP-E224A	N671	A to C	GGCAAAAGCTCTATGCGTTCCGGAGAGG,
			CCTCTCCGGAACGCATAGAGCTTTTGCC
GFP-F225A	N673-674	TT to GC	GCAAAAGCTCTATGAGGCCCGGAGAGGGATGAA,
			TTCATCCCTCTCCGGGCCTCATAGAGCTTTTGC
GFP-R226A	N676-677	CG to GC	CAAAAGCTCTATGAGTTCGCGAGAGGGATGAAAAGGTATG,
			CATACCTTTTCATCCCTCTCGCGAACTCATAGAGCTTTTG
GFP-R227A	N679-680	AG to GC	AAAAGCTCTATGAGTTCCGGGCAGGGATGAAAAGGTATGT,
			ACATACCTTTTCATCCCTGCCCGGAACTCATAGAGCTTTT
GFP-RR	N676-677	CG to GC	GGGCAAAAGCTCTATGAGTTCGCTGCAGGGATGAAAAGGTATGTGAC,
	N679-680	AG to GC	GTCACATACCTTTTCATCCCTGCAGCGAACTCATAGAGCTTTTGCCC
GFP-G228A	N683	G to C	CTATGAGTTCCGGAGAGCGATGAAAAGGTATGTG,
			CACATACCTTTTCATCGCTCTCCGGAACTCATAG
GFP-S250A	N748	T to G	CCTCTGCGCCGCCAGTAACACCGAG,
			CTCGGTGTTACTGGCGGCGCAGAGG
GFP-S251A	N751-752	AG to GC	CTCTGCGCCTCCGCTAACACCGAGACG,
			CGTCTCGGTGTTAGCGGAGGCGCAGAG

Table 1 Site-directed mutagenesis of human WIPI-1 *(Continued)*

GFP-T255A	N763	A to G	CCAGTAACACCGAGGCGGTACACATCTTC, GAAGATGTGTACCGCCTCGGTGTTACTGG
GFP-H257A	N769-770	CA to GC	CACCGAGACGGTAGCCATCTTCAAGCTGGAAC, GTTCCAGCTTGAAGATGGCTACCGTCTCGGTG
GFP-S335A	N1003-1004	AG to GC	GCTAGTTGCGTCATCCGCTGGACACCTTTATATG, CATATAAAGGTGTCCAGCGGATGACGCAACTAGC
GFP-G336A	N1007	G to C	CTAGTTGCGTCATCCAGTGCACACCTTTATATG, CATATAAAGGTGTGCACTGGATGACGCAACTAG

Table S1; Additional file 4: Figure S3) and representative confocal images are presented (Additional file 5: Figure S4). From this, the quantification of puncta-positive cells upon RM administration along with p-value calculations is provided in Figure 2. With regard to wild-type GFP-WIPI-1, RM administration resulted in a significant reduction in the number of puncta-positive cells when the following mutants were expressed: R112A, H185A, G198A, S203A, S205A, G208A, T209A, R212A, F225A, R226A, R227A, G228A, S251A, T255A, H257A. Within this group, the following mutants were unable to form puncta: S203A, S205A, G208A, T209A, R212A, R226A, R227A, G228A, S251A, T255A, H257A. Exceptional, the expression of the R110 mutant resulted in an increased number of puncta-positive cells. The expression of the following mutants did not result in a significant alteration in puncta formation with regard to wild-type GFP-WIPI-1: N23A, Q24A, D25A, E64A, R107A, E224A, S250A, S335A, G336A (Figure 2, Additional file 3: Table S1, Additional file 4: Figure S3).

We extended this analysis and transiently expressed wild-type GFP-WIPI-1 or either of the mutants in human G361 cells that also express high levels of endogenous WIPI-1. The quantification (n = 3) of GFP-

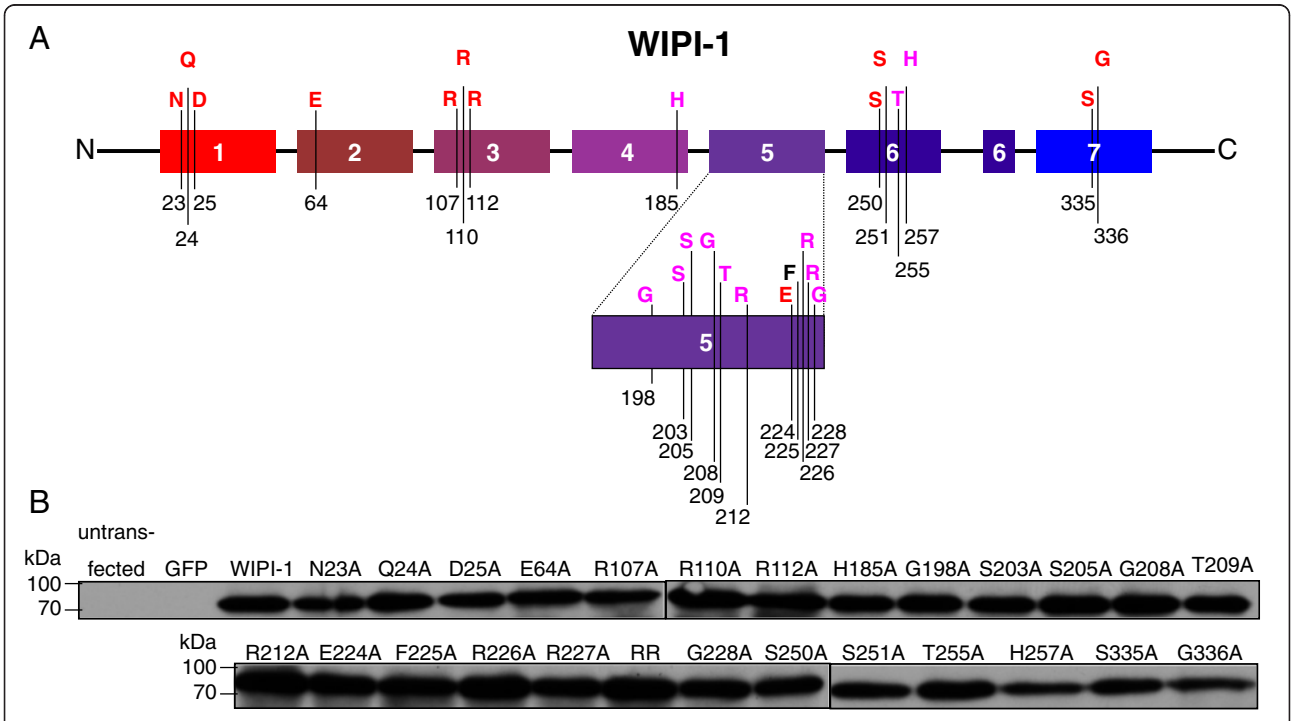

Figure 1 Generation and transient expression of GFP-WIPI-1 mutants in human U2OS cells. (A) Representation of the human WIPI-1 protein harbouring 7 WD repeats (coloured boxes 1–7) and evolutionarily conserved amino acids (homologous amino acids in red, invariant amino acids in purple, not conserved residue in black). **(B)** Transient over-expression and anti-GFP ECL analysis of GFP-tagged wild-type WIPI-1 (labelled WIPI-1) or generated mutant WIPI-1 variants (labelled N23A – G336) along with the GFP control and untransfected U2OS cells. The RR mutant carries alanine substitutions for both R226 and R227. Supplementary material provides an amino acid sequence alignment of wild-type and mutant WIPI-1 variants deduced from automated DNA sequencing upon site-directed mutagenesis (Additional file 1: Figure S1).

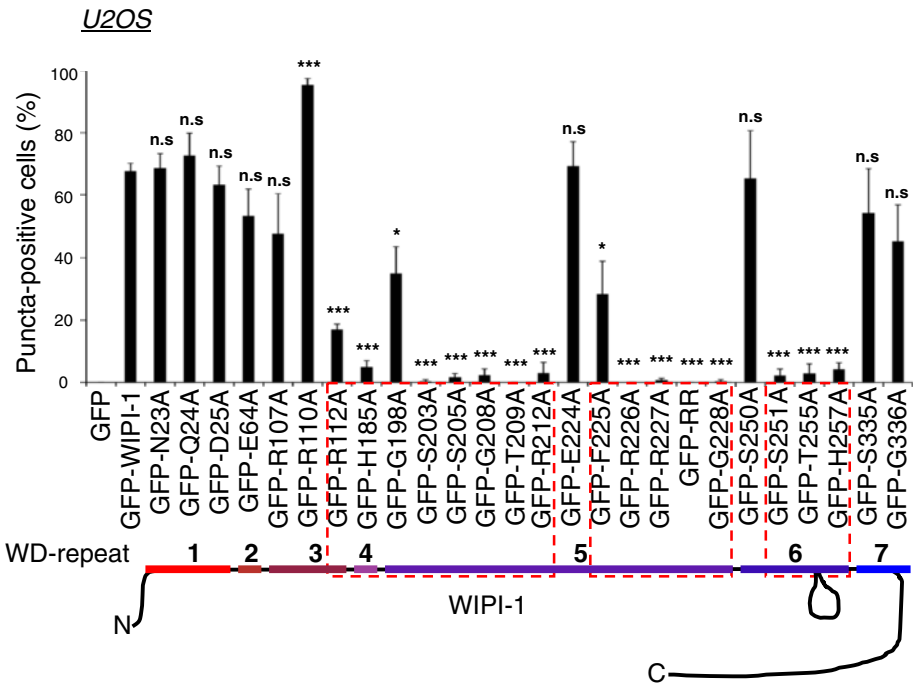

Figure 2 Quantitative puncta-formation analysis of GFP-tagged wild-type or mutant WIPI-1 variants in U2OS cells. U2OS cells transiently expressing GFP-WIPI-1 or GFP-tagged mutant WIPI-1 variants were treated for 3 h with control medium (CM), 233 nM wortmannin (WM), 300 nM rapamycin (RM), or rapamycin plus wortmannin (RM/WM), fixed and analyzed by confocal laser-scanning microscopy. Representative images and quantifications from all treatments are provided (Additional file 3: Table S1, Additional file 4: Figure S3, Additional file 5: Figure S4). From this, the quantification of rapamycin-treated cells is presented here as the percentage of puncta-positive cells for wild-type and mutant GFP-WIPI-1 variants (300 cells per condition, n = 3). P-values (reference GFP-WIPI-1): n.s. ≥ 0.05, * < 0.05, *** < 0.001.

WIPI-1 wild-type or mutant puncta-positive cells was performed upon RM administration in 300 individual cells (Additional file 6: Table S2) and p-value calculations conducted with regard to wild-type GFP-WIPI-1 (asterisks) or with regard to the number of puncta-positive cells achieved in U2OS cells (number sign) (Figure 3). Clearly, the expression of wild-type GFP-WIPI-1 or either of the puncta-formation competent mutants in G361 cells followed by rapamycin administration resulted in a significant increase in the number of puncta-positive G361 cells when compared to U2OS cells (Figure 3, number signs). In contrast to U2OS cells, the G198A mutant no longer showed a reduction in the number of puncta-positive cells when compared with wild-type GFP-WIPI-1 (Figure 3). All of the other mutants expressed in G361 cells (Figure 3) showed similar results when compared to U2OS cells (Figure 2).

To detail the puncta analysis of mutant GFP-WIPI-1 proteins where the particular alanine substitution did not nullify the ability to localize at autophagosomal membranes (fluorescent puncta), we visualized this group of mutants (N23A, Q24A, D25A, E64A, R107A, R110A, R112A, G198A, E224A, F225A, S250A, S335A, G336A) or wild-type GFP-WIPI-1 (green) along with endogenous Atg12 (red) upon rapamycin-induced autophagy. Representative confocal images are presented, demonstrating that wild-type GFP-WIPI-1 as well as the mutants capable of puncta-formation co-localized (yellow) with Atg12 at perinuclear structures, reflecting ER-associated phagophore membranes (Figure 4). WIPI-1 mutants found to be incompetent for PtdIns(3)P binding were distributed throughout the cytoplasm and did not co-localize with formed Atg12 puncta upon rapamycin-mediated mTORC1 inhibition (data not shown).

During quantitative confocal microscopy it became apparent that the R110A puncta structures differed from wild-type GFP-WIPI-1 puncta. The R110A mutant showed a significant increase in the number of puncta-positive cells in all of the treatments (CM, WM, RM, RM/WM) when compared to wild-type GFP-WIPI-1 in U2OS cells. In addition, wortmannin did not abolish the ability to form distinct intracellular puncta (Figure 5A, Additional file 3: Table S1, Additional file 4: Figure S3). In order to compare the R110A puncta structures with wild-type GFP-WIPI-1, we distinguished between four categories of characteristic cytoplasmic WIPI-1 puncta appearing upon the induction of autophagy [29,39]: large elongated perinuclear structures (category 1), large lasso-like structures (category 2), large circular structures/vesicles (category 3), small dots (category 4)

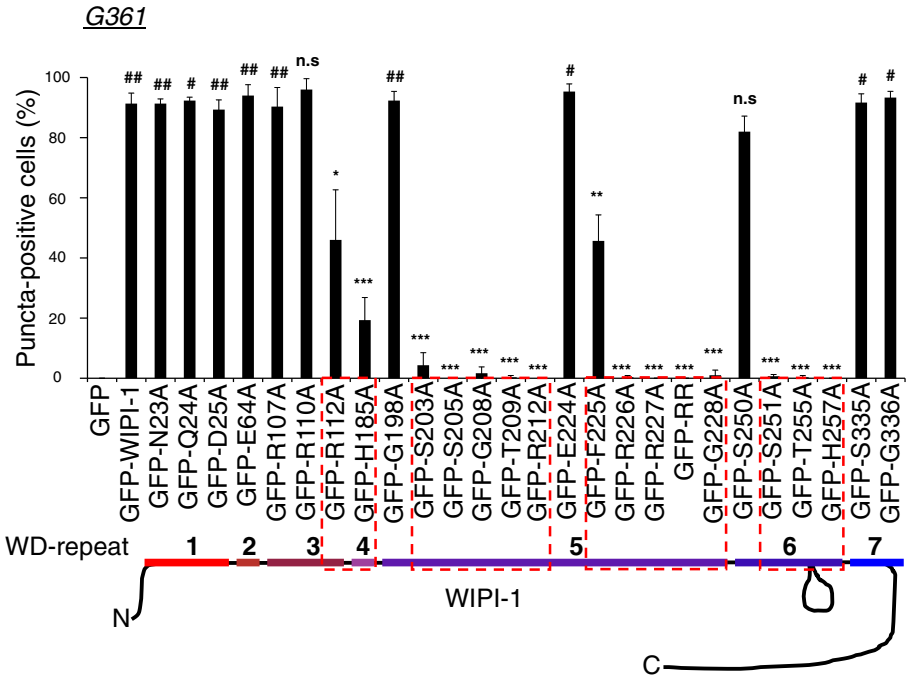

Figure 3 Quantitative puncta-formation analysis of GFP-tagged wild-type or mutant WIPI-1 variants in G361 cells. G361 cells transiently expressing GFP-WIPI-1 or GFP-tagged mutant WIPI-1 variants were treated for 3 h with 300 nM rapamycin (RM), fixed and analyzed by confocal laser-scanning microscopy. Quantifications (Additional file 6: Table S2) are presented as the percentage of puncta-positive cells for wild-type and mutant GFP-WIPI-1 variants (300 cells per condition, n = 3). P-values with regard to GFP-WIPI-1: n.s. ≥ 0.05, * < 0.05, ** < 0.01, *** < 0.001. *P*-values with regard to the corresponding condition in U2OS cells: # < 0.05, ## < 0.01.

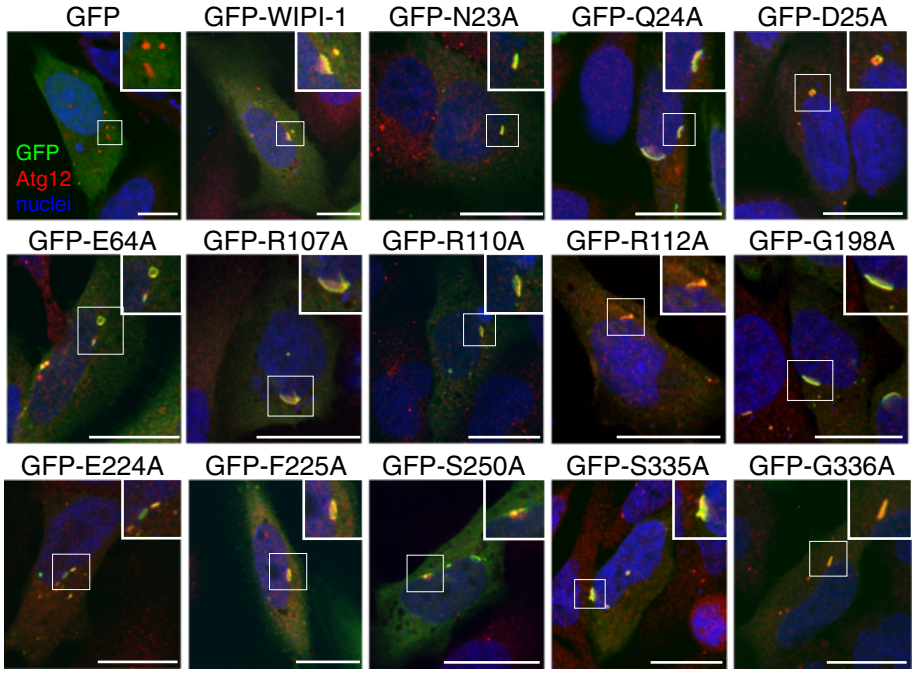

Figure 4 Colocalization of endogenous Atg12 with wild-type GFP-WIPI-1 and puncta-formation competent GFP-WIPI-1 mutants upon rapamycin-mediated induction of autophagy. U2OS cells transiently expressing GFP-WIPI-1 or GFP-tagged mutant WIPI-1 variants were treated for 3 h with 300 nM rapamycin, fixed, stained with anti-Atg12/Alexa 546 antibodies (red) and TOPRO3 (nuclei, blue), and analyzed by confocal laser-scanning microscopy. Merged images are shown. Scale bars 20 μM.

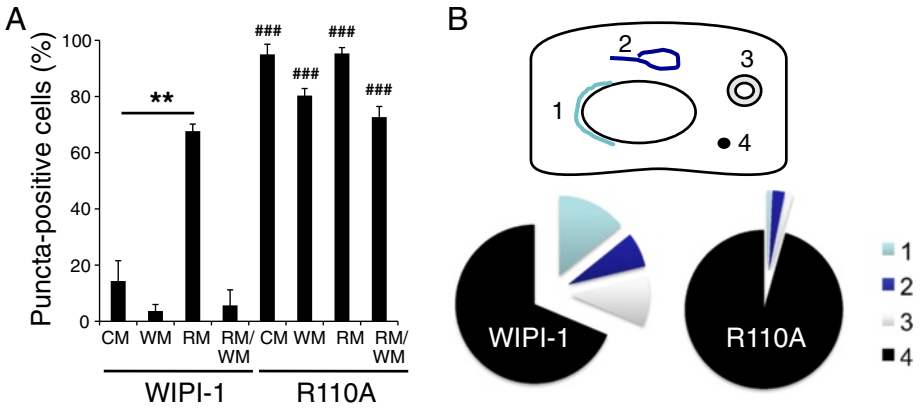

Figure 5 Puncta analysis of the R110A mutant. (A) P-value calculation for quantitative R110A puncta-formation analysis (Additional file 3: Table S1, Additional file 4: Figure S3, Additional file 5: Figure S4) with regard to CM: ** < 0.01; with regard to wild-type GFP-WIPI-1: ### < 0.001. **(B)** 50 puncta structures of GFP-WIPI-1 or GFP-R110A were categorized (1–4). Further supplementary material is available (Additional file 7: Figure S5).

(Figure 5B). According to these four categories we quantified the puncta structures in GFP-WIPI-1 wild-type and R110A cells upon rapamycin administration. Predominantly, R110A puncta appeared as small cytoplasmic dots of category 4 (95.57%) and only a minority of puncta (4.43%) as large puncta of categories 1–3. In contrast, 31.295% of wild-type GFP-WIPI-1 puncta-positive cells showed large structures (categories 1–3) and 68.705% small cytoplasmic dots (category 4) (Figure 5B, Additional file 7: Figure S5). By applying this puncta analysis to further alanine mutants of conserved amino acids that cluster across the top of the propeller blades 1–3 in WIPI-1, we also found that a decrease of large puncta formation was apparent when D24, E64, R107 and R112 mutants were expressed in U2OS cells (Additional file 7: Figure S5).

To analyze the generated GFP-WIPI-1 mutants in their ability to bind PtdIns(3)P and PtdIns(3,5)P_2, we first confirmed that over-expressed wild-type GFP-WIPI-1 in different cell lines that either express detectable (G361) or undetectable (HeLa, U2OS) levels of endogenous WIPI-1 protein (Figure 6A), predominantly binds PtdIns(3)P and to a minor extend PtdIns(3,5)P_2 (Figure 6B and 6C upper panel). As expected, the RR

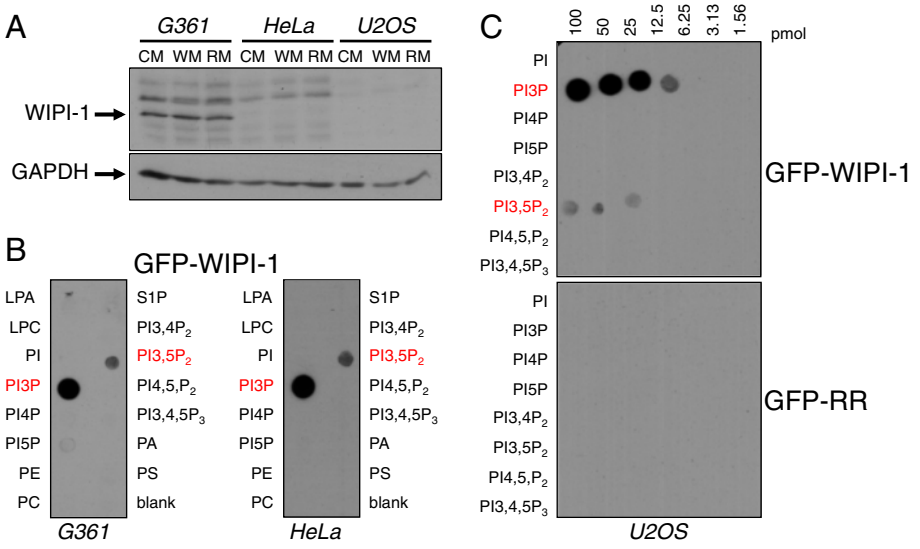

Figure 6 GFP-WIPI-1 binding to PtdIns(3)P and PtdIns(3,5)P_2. (A) Western blot analysis of endogenous WIPI-1 protein in G361, HeLa or U2OS cells upon treatments with control medium (CM), 233 nM wortmannin (WM) or 300 nM rapamycin (RM). **(B)** Transient over-expression of GFP-WIPI-1 in G361 (left panel) or HeLa (right panel) cells followed by protein-phospholipid overlay assays using native cell extracts, adjusted to contain equivalent levels of GFP-WIPI-1 protein. **(C)** Protein-phospholipid overlay assay using native cell extracts from GFP-WIPI-1 or GFP-RR expressing U2OS cells.

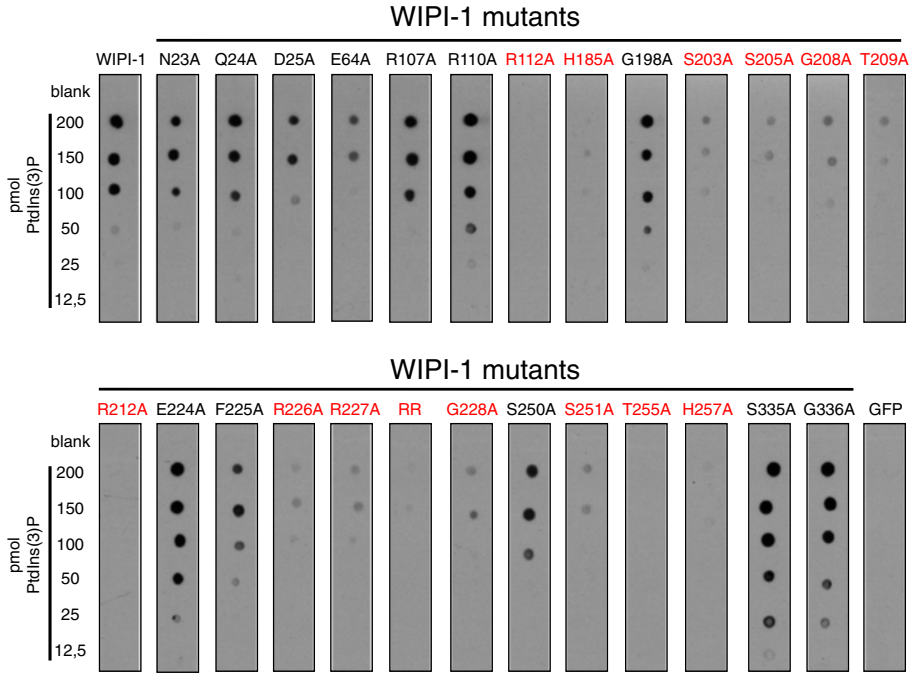

Figure 7 Protein-phospholipid overlay assays with wild-type and mutant GFP-WIPI-1 variants. From U2OS cells transiently expressing GFP-WIPI-1 or GFP-tagged mutant WIPI-1 variants native cell extracts were generated in parallel and used to overlay membrane-immobilized PtdIns(3)P (12,5–200 pmol) followed by anti-GFP ECL detection. Prior to overlaying the membranes with native cell extracts, the volumes of the different extracts were adjusted to include equivalent levels of GFP-WIPI-1 wild-type or mutant protein, judged by anti-GFP western blotting (not shown). Representative results are shown (n = 3). In red, GFP-tagged WIPI-1 mutants unable to bind to PtdIns(3)P.

mutant (R226A/R227A) did not bind to either of the phospholipids (Figure 6C lower panel).

By using different concentrations of immobilized PtdIns(3)P (12.5–200 pmol), protein-phospholipid overlay assays (n = 3) were conducted with transiently overexpressed GFP-WIPI-1 mutants along with wild-type GFP-WIPI-1 as a positive and GFP as a negative control from native U2OS cell extracts (Figure 7). Of note, equal GFP-WIPI-1 wild-type or mutant protein levels in native cell extracts used for protein-phospholipid overlay assays were adjusted upon western blot analysis (data not shown). Likewise, the mutants unable to form puncta

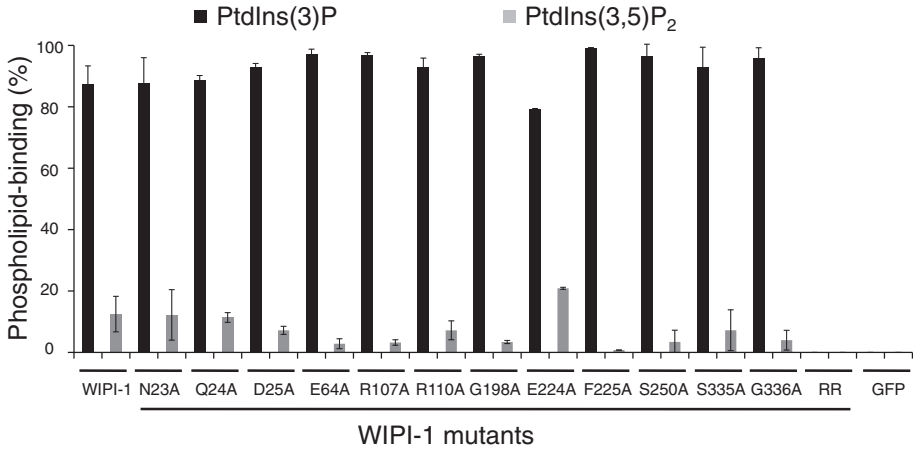

Figure 8 GFP-WIPI-1 mutants capable of PtdIns(3)P can also bind to PtdIns(3,5)P_2. Quantification of phospholipid-protein overlay assays using membrane-immobilized PtdIns(3)P and PtdIns(3,5)P_2, and native cell extracts from U2OS cells transiently expressing GFP-tagged wild-type or mutant WIPI-1 variants (n = 2). Total intensities of anti-GFP ECL signals at PtdIns(3)P and PtdIns(3,5)P_2 positions were set to 100% for each variant and the very approximate percentage of PtdIns(3)P and PtdIns(3,5)P_2 binding calculated.

Table 2 Characterization of WIPI-1 mutants

WIPI-1 Mutant	Puncta formation	PtdIns(3)P binding	PtdIns(3,5)P_2 binding	Atg12 colocalization
GFP-N23A	+	+	+	+
GFP-Q24A	+	+	+	+
GFP-D25A	+	+	+	+
GFP-E64A	+	+	+	+
GFP-R107A	+	+	+	+
GFP-R110A	+	+	+	+
GFP-R112A	+	-	n/a	+
GFP-H185A	+	-	n/a	n/a
GFP-G198A	+	+	+	+
GFP-S203A	-	-	-	-
GFP-S205A	-	-	-	-
GFP-G208A	-	-	-	-
GFP-T209A	-	-	-	-
GFP-R212A	-	-	-	-
GFP-E224A	+	+	+	+
GFP-F225A	+	+	+	+
GFP-R226A	-	-	-	-
GFP-R227A	-	-	-	-
GFP-RR	-	-	-	-
GFP-G228A	-	-	-	-
GFP-S250A	+	+	+	+
GFP-S251A	-	-	-	-
GFP-T255A	-	-	-	-
GFP-H257A	-	-	-	-
GFP-S335A	+	+	+	+
GFP-G336A	+	+	+	+

(Figure 2, Figure 3) were unable to bind PtdIns(3)P (Figure 7, highlighted in red). In addition, the R112A and H185A mutants with reduced puncta-formation ability were also unable to bind PtdIns(3)P (Figure 7, highlighted in red). Further, mutants unable to bind to PtdIns(3)P did also not bind to PtdIns(3,5)P_2 (data not shown). From the group of mutants able to bind PtdIns (3)P and PtdIns(3,5)P_2, we addressed the very approximate PtdIns(3)P: PtdIns(3,5)P_2 binding ratio. Using GFP-WIPI-1 as a positive and both the RR mutant and GFP as negative controls, we conducted protein-phospholipid overlay assays with immobilized PtdIns(3)P and PtdIns(3,5)P_2 on the same membrane (data not shown). Based on anti-GFP ECL densitometry we calculated the approximate percentage of bound GFP-WIPI-1 to either of the phospholipids (Figure 8, n = 2). This result indicated that the mutants tested did not show key differences in their approximate PtdIns(3)P: PtdIns(3,5)P_2 binding ability when compared to wild-type GFP-WIPI-1 (Figure 8).

The results achieved from characterizing the generated mutant GFP-WIPI-1 proteins are summarized in Table 2. From this analysis it became apparent that the evolutionarily conserved residues located in propeller blades 5 and 6 should fold into a 3-dimensional motif to confer direct PtdIns binding. Of note, propeller blade 5 and 6 sequences represent the most homologous protein region within the WIPI protein family, as shown by bioinformatic cluster analysis (Figure 9).

As we employed rapamycin-mediated mTORC1 inhibition to induce autophagy for the characterization of the generated WIPI-1 mutants, we functionally addressed if siRNA-mediated downregulation of mTOR (Figure 10A) would likewise result in an increase of WIPI-1 puncta-positive cells. For this aim we used our previously established automated fluorescent puncta-image acquisition (Figure 10B) and analysis (Figure 10C) platform upon siRNA transfections of stable GFP-WIPI-1 U2OS cells. Clearly, down regulation of mTOR resulted in a significant increase of both GFP-WIPI-1 puncta-positive cells (Figure 10C, left panel) and puncta per individual cell (Figure 10C, right panel). In the presence of RM these levels further increased, and decreased in the presence of WM (Figure 10C).

To confirm that the function of WIPI-1 at the onset of autophagy reflects its binding to generated PtdIns(3)P rather than to PtdIns(3,5)P_2, we employed the compound YM201636 (YM) to specifically block PtdIns(3,5)P_2 production by PIKfyve-mediated phosphorylation of PtdIns(3)P [40]. YM was added to control medium (CM), FCS-free CM or nutrient-free medium (NF) lacking both amino acids and FCS. WM was employed in parallel to inhibit PtdIns(3)P generation. Endogenous WIPI-1 was visualized by indirect immunofluorescence and the number of WIPI-1 puncta-positive cells was determined from a total of 150 individual cells for each condition (n = 3) (Figure 11A). In CM, the addition of YM resulted in an increase of WIPI-1 puncta-positive cells, indicating that indeed, PtdIns(3)P is bound by WIPI-1 at autophagosomal membranes. Further, by analyzing shRNA-mediated down regulation of WIPI-1 in G361 we confirmed that the PtdIns(3)P-effector function of WIPI-1 is essential for LC3 lipidation at the onset of autophagy (Figure 11B) [32].

Discussion

Using quantitative WIPI-1 puncta-formation analysis we functionally identified critical amino acids for PtdIns(3)P-mediated autophagosomal membrane binding of human WIPI-1 (Figure 12) downstream of mTORC1 inhibition and PtdIns3KC3 activation (Figure 13). We found that the residues S203, S205, G208, T209, R212,

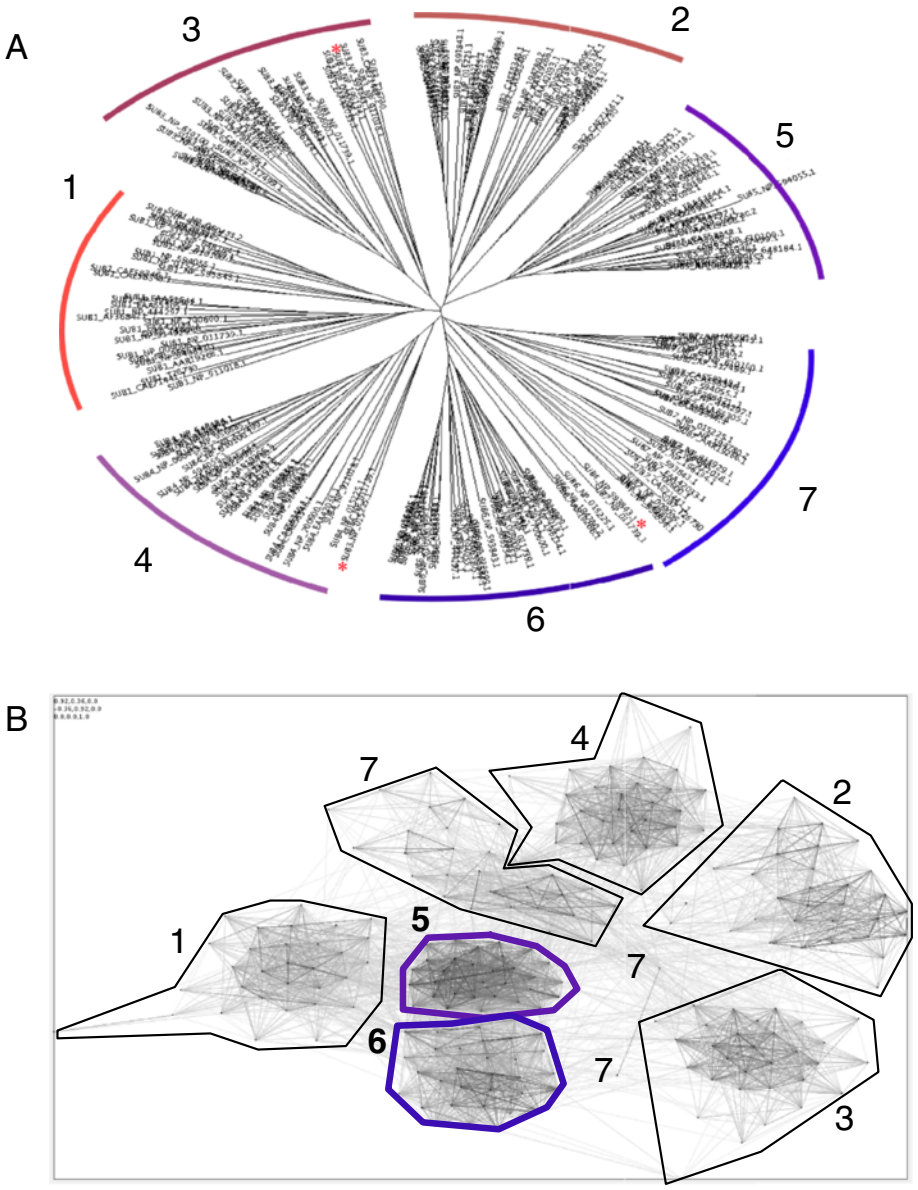

Figure 9 Bioinformatic analysis of WIPI propeller blades. (A) Phylogenetic and **(B)** cluster analysis of individual (1–7) beta-propeller blade sequences of the WIPI protein family [29].

R226, R227, G228, S251, T255, H257 (Figure 12, highlighted with green bars), displaying a cluster across propeller blades 4–7 [29], are responsible for PtdIns (3)P-binding at autophagosomal membranes during auto-phagy initiation. In line, a subset of this group of residues (Figure 12, highlighted in red lettering) was recently identified to provide PtdIns-binding of HSV2, a yeast homolog of human WIPI-1 via two binding sites [30] (Figure 12, site 1, site 2). These critical residues are predominantly positioned on propeller blade 5 and 6 of human WIPI-1 (Figure 12), both of which we show to be the most homologous propeller blades throughout the WIPI protein family (Figure 9B). Because the WIPI propeller was differentiated into its seven blades at the time when both paralogous groups of the WIPI protein family evolved ([29], Figure 9A), the ancestral function of WIPI proteins should be crucially defined by PtdIns-binding properties. Of note, puncta-formation and PtdIns(3)P-binding competent WIPI-1 mutants also bound to a minor extend to PtdIns(3,5)P_2 as earlier found for wild-type WIPI-1 and WIPI-2 [24,36,37], demonstrating that identical amino acids confer binding to PtdIns(3)P or PtdIns(3,5)P_2. The proposed binding of HSV2 to two phosphoinositides simultaneously (Figure 12, site 1, site 2) could lead to a simultaneous PtdIns(3)P/PtdIns(3,5)P_2 binding of the WIPI propeller under certain

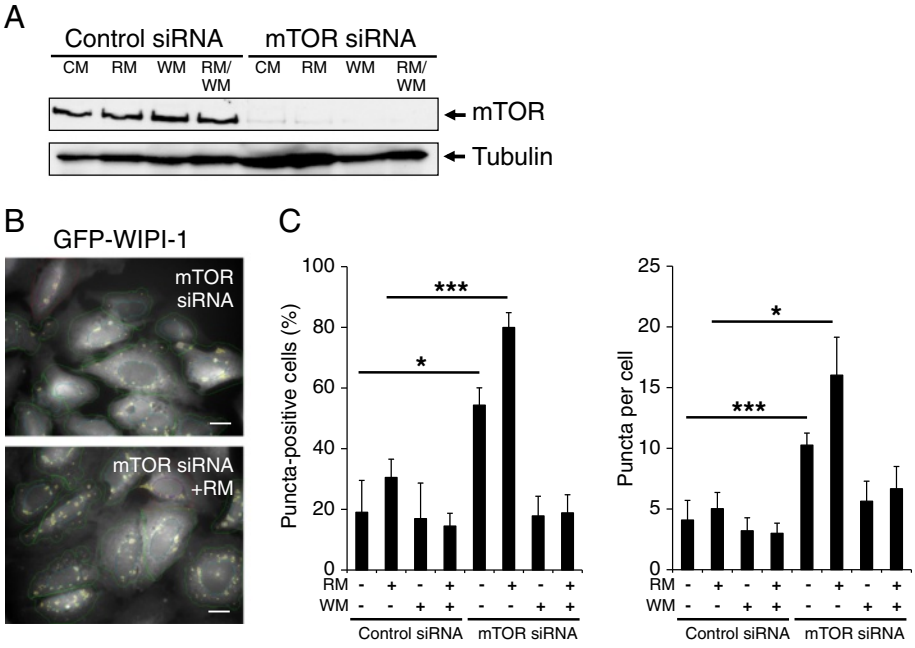

Figure 10 Downregulation of mTOR elevates the number of cells that display GFP-WIPI-1 puncta. (A) Human U2OS cells stably expressing GFP-WIPI-1 were transfected with 20 nM control siRNA or siRNA targeting mTOR. 48 h post-transfection the cells were treated with control medium (CM), rapamycin (RM), wortmannin (WM) or rapamycin plus wortmannin (RM/WM) for 2 h, and a representative western blot analysis from 3 independent experiments confirmed mTOR down regulation. **(B)** Fluorescence images were automatically acquired and **(C)** analyzed, and results (600–800 cells per condition, n = 3) expressed as GFP-WIPI-1 puncta-positive cells (left panel) or GFP-WIPI-1 puncta per cell (right panel). P-values: * < 0.05, *** < 0.001. Scale bars 20 μM.

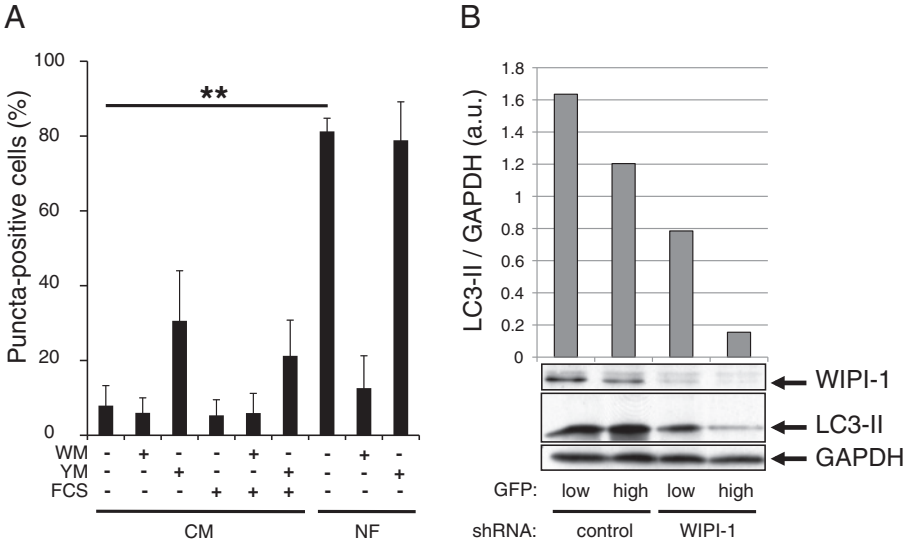

Figure 11 PIKfyve inhibition elevates the number of cells that display WIPI-1 puncta, and WIPI-1 downregulation decreases LC3 lipidation. (A) Human G361 cells were treated for 3 h either with YM201636 (YM) or wortmannin (WM) diluted in complete control medium (CM) with or without serum (FCS) or in serum- and amino acid-free medium (NF), followed by immunostaining of endogenous WIPI-1 using anti-WIPI-1/Alexa 488 antibodies and quantitative fluorescence microscopy. Results are expressed as the number of WIPI-1 puncta-positive cells (150 cells per condition, n = 3). P-value: ** < 0.01. **(B)** G361 cells were transfected with GFP-labelled control shRNA or shRNA targeting WIPI-1, and GFP-expressing cells were sorted into two groups with regard to high or low GFP intensities. Anti-WIPI-1 and anti-LC3 ECL analysis was conducted and signal intensities normalized over GAPDH. Representative results are shown (n = 2).

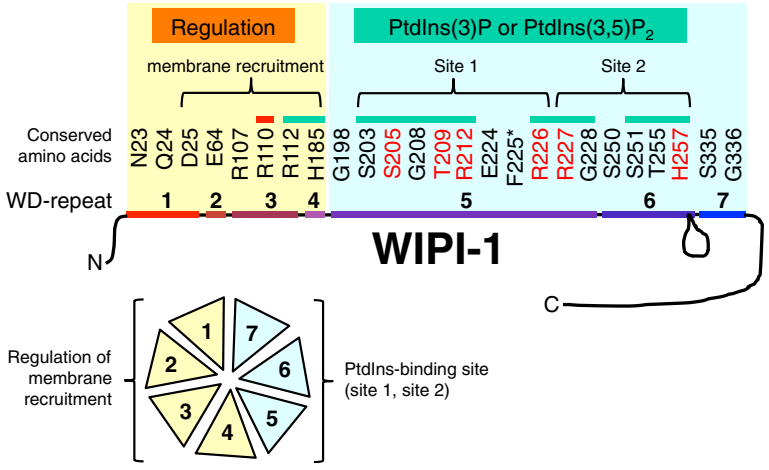

Figure 12 Graphical interpretation of the results achieved from the analysis of generated WIPI-1 mutants. See discussion for details.

circumstances. Hence phosphorylation of PtdIns(3)P to generate PtdIns(3,5)P_2 could regulate the function of WIPI proteins as PtdIns effectors. However, since WIPI-1 puncta formation is elevated when PtdIns(3,5)P_2 production is blocked (Figure 11A), the specific localization at autophagosomal membranes upon autophagy induction should indeed predominantly reflect PtdIns(3)P binding of WIPI-1.

In addition to the residues conferring PtdIns(3)P binding, two residues, R112 and H185, (Figure 12, highlighted with green bars) were unable to efficiently bind PtdIns(3) but to localize at Atg12-positive autophagosomal membranes, in particular when expressed in cells with high levels of endogenous WIPI-1. This strongly indicates that membrane recruitment is mediated by evolutionarily conserved protein-protein interactions that regulate specific membrane localization of WIPI proteins. Further, one particular residue, R110, might be responsible for the association of an as yet unidentified inhibitory factor, as membrane localization was independent of autophagy stimulation and insensitive to autophagy inhibition (Figure 12, highlighted with a red bar). From this we suggest that the amino acids of propeller blades 1–4 provide differential association sites for regulatory factors that confer specific membrane binding, and amino acids of propeller blades 5–7 direct PtdIns binding. In line, by investigating the co-localization of WIPI-1 and the FYVE

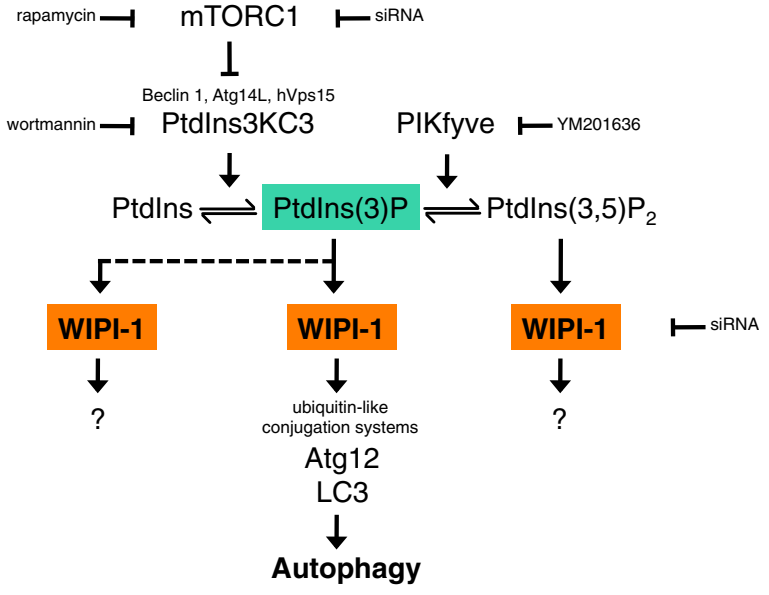

Figure 13 A model for the role of WIPI-1 as a PtdIns(3)P effector at the onset of autophagy in human tumour cells. As indicated, different compounds and siRNA's have been used in this study. See discussion for details.

domain (GFP-2xFYVE) that also binds PtdIns(3)P, we show that WIPI-1 and GFP-2xFYVE did not prominently colocalize at same membranes upon rapamycin-mediated autophagy (Additional file 8: Figure S6), further indicating that the specificity of WIPI-1 to localize at autophagosomal membranes should indeed be directed by regulatory interacting factors.

Conclusions

Evolutionarily conserved residues in WIPI-1 functionally identified in this study should confer specific binding to i) PtdIns(3)P or PtdIns(3,5)P_2 and to ii) conserved interacting factors that determine membrane recruitment and specificity (Figure 12). Our study further provides evidence that the PtdIns(3)P effector function of WIPI-1 is regulated downstream of mTORC1 inhibition and PtdIns3KC3 activation, and upstream of both Atg12 and LC3 conjugation systems (Figure 13). By binding to PtdIns(3)P or PtdIns(3,5)P_2, we anticipate that WIPI-1 might also be involved in additional as yet unidentified functions (Figure 13).

Methods

Reagents

Rapamycin, wortmannin and YM201636 were obtained from Sigma-Aldrich; Bafilomycin A_1 from Applichem; PIP strips, PIP arrays, D-*myo*-phosphatidylinositol-3-phosphate, D-*myo*-phosphatidylinositol-3,5-bisphosphate from Echelon Biosciences.

Primary antibodies

Anti-GFP antibody was purchased from Roche, anti-Atg12L antiserum from Abgent, anti-LC3 antibody from Nanotools, anti-α-tubulin antibody from Sigma-Aldrich, anti-GAPDH antibody from HyTest, anti-mTOR from Cell Signaling. The rabbit polyclonal anti-WIPI-1 antiserum was described earlier [29].

Secondary antibodies

Alexa Fluor 488 and Alexa Fluor 546 goat anti-mouse and anti-rabbit IgG antibodies were obtained from Invitrogen, anti-mouse IgG-HRP and anti-rabbit IgG-HRP antibodies from GE Healthcare.

Fluorescent dyes

TO-PRO-3 was obtained from Invitrogen and DAPI was purchased from AppliChem.

cDNA constructs

GFP-WIPI-1 (pEGFP.C1-WIPI-1α) [29] was used as DNA template for site-directed mutagenesis (Quick change II, Stratagene) to generate GFP-WIPI-1 mutants with synthesized (Purimex, Sigma-Aldrich) oligonucleotides (see Table 1). Construct integrities were verified by DNA sequencing.

Cell culture and transfection

Human U2OS and G361 cells (both from ATCC) were cultured in DMEM, 10% FCS, 100 U/ml penicillin/100 μg/ml streptomycin, 5 mg/ml plasmocin (Invivogen) at 37°C, 5% CO_2. The monoclonal U2OS cell line stably expressing GFP-WIPI-1 was described earlier [41] and cultured in the presence of 0.6 mg/ml G418 (Invitrogen). Cells were transfected with DNA using PromoFectin (Promocell) or Lipifectamine2000 (Invitrogen) according to the manufacturer's instruction. Using RNAiMax (Invitrogen) 20 nM control siRNA or siRNA targeting mTOR (both from Cell Signalling) were transfected according to the manufacturer's instruction for reverse transfection. Using Lipofectamine2000 G361 cells were transfected with shRNA constructs targeting human WIPI-1 and expressing GFP (SuperArray), followed by fluorescence-assisted cell sorting [42] of low or high GFP-expressing cells.

Autophagy assays

Autophagy assays were conducted for 2 or 3 h using amino acid and serum-free medium (EBSS, from Sigma Aldrich), and by administration of rapamycin (300 or 500 nM), wortmannin (233 nM) or YM201636 (800 nM).

Confocal laser-scanning microscopy

Cells were fixed (3.7% paraformaldehyde in PBS) and prepared for direct fluorescence of GFP-WIPI-1 or for indirect immunofluorescence of endogenous WIPI-1 or Atg12 using anti-WIPI-1 or anti-Atg12 antiserum at 1:25–1:50 and Alexa Fluor secondary antibody conjugates (Alexa 488 or Alexa 546) at 1:200–1:250. Z-stacks (10–20 optical sections of 0.5 μm) were acquired using Zeiss/Axiovert 100 M/LSM510 and a 63 × 1.4 DIC Plan-apochromat objective. Individual optical sections were used to analyse co-localization events. Projections of individual optical sections were used to generate final images.

Automated high throughput GFP-WIPI-1 punctaformation image acquisition and analyses

Stable U2OS GFP-WIPI-1 cells were cultured in 6 well plates, transfected with 20 nM siRNA's and 48 h post-transfection autophagy assays were performed for 2 h. Cells were fixed (3,7% PFA in PBS) and incubated with DAPI (5 μg/ml PBS). Using a high content platform (In Cell Analyzer 1000, GE Healthcare) equipped with a Nikon Plan Fluor ELWD 40 × 0,6 objective, automated GFP-WIPI-1 image acquisition and analysis (In Cell Analyzer Workstation 3.4) was conducted as previously described [41].

Immunoblotting

Cells were lysed in hot Laemmli buffer and total protein extracts used for standard western blotting and ECL detection (GE Healthcare). Protein abundance was normalized over GAPDH by quantifying ECL signal intensities using the Personal Densitometer SI (Molecular Dynamics) and Image Quant 5.1.

Phospholipid-protein overlay assay

Phosphatidylinositol-3-phosphate diC16 and Phosphatidylinositol-3,5-bisphosphate diC16 were solved in 1:2:0,8 $CHCl_3$: MeOH: H_2O and applied on a nitrocellulose membrane (Amersham Hybond™-C Extra). Membrane-immobilized phospholipids were dried at room temperature in the dark for 1 h. Alternatively, PIP strips or PIP arrays (Echelon Biosciences) were used. As described earlier [37], membrane-immobilized phospholipids were rinsed in TBS and TBS/0.1% Tween, and blocked for 1 h at room temperature in TBS/0.1% Tween/3% BSA. Membranes were incubated with the soluble fractions (50 μg to 150 μg total protein) from native cell extracts (750 mM aminocaproic acid, 50 mM Bis-Tris, 0.5 mM EDTA, pH 7.0, Roche Protease inhibitor Cocktail) for 16 h at 4°C. Prior to this incubation step, aliquots of the soluble fractions were used for Bradford assays and to normalize protein expression by western blotting and densitometry. From this, native extract volumes were adjusted to contain equivalent levels of over-expressed proteins (wild-type GFP-WIPI-1 and the generated mutants). Finally, anti-GFP ECL detection was used to detect phospholipid-bound proteins.

Statistical analysis

Mean values from 3 independent sets of experiments (± SD) were used to calculate p-values (heteroscedastic t-testing).

Bioinformatics

Individual beta-propeller blade sequences of the WIPI protein family were analysed phylogenetically using CLANS cluster analysis [43] and ASATURA neighbor-joining phylogeny [44] as previously described [29].

Additional files

Additional file 1: Figure S1. Multiple amino acid sequence alignment of wild-type human WIPI-1 and generated mutants. Yellow: alanine substitutions of homologous residues within the WIPI protein family, red: alanine substitutions of invariant residues, green: alanine substitution of a nonhomologous residue.

Additional file 2: Figure S2. LC3-lipidation analysis upon rapamycin-mediated autophagy in U2OS cells. Control U2OS cells or U2OS cells transiently expressing GFP-WIPI-1 were treated with rapamycin in the presence or absence of protease inhibitors (P.I.) followed by anti-LC3 western blot analysis from total protein extracts. The LC3-II/LC3-I ratio was determined by densitometry.

Additional file 3: Table S1. Quantitative GFP-WIPI-1 puncta-formation analysis in U2OS cells. Treatments: control medium (CM), rapamycin (RM), rapamycin plus wortmannin (RM/WM), wortmannin (WM). The number of puncta-positive cells was determined in 100 cells per condition. The data from three independent experiments (dataset 1–3) along with mean values (%) is presented.

Additional file 4: Figure S3. Graphical representation of the results provided in Additional file 3: Table S1 along with standard deviations. In addition, the number for non-puncta cells is also presented for each condition. In black: puncta-positive cells, in white: non-puncta cells.

Additional file 5: Figure S4. Representative confocal images from the analysis provided in Additional file 3: Table S1. Bars: 20 μM.

Additional file 6: Table S2. Quantitative GFP-WIPI-1 puncta-formation analysis in G361 cells. Treatment: rapamycin (RM). The number of puncta-positive cells was determined in 100 cells per dataset (1–3). Original data and mean values (%) are presented.

Additional file 7: Figure S5. The percentage of small and large puncta structures displayed by wild-type and mutant GFP-WIPI-1 proteins upon rapamycin administration in U2OS cells. Images from Additional file 5: Figure S4 were used and 50 puncta structures were categorized for each GFP-WIPI-1 mutant.

Additional file 8: Figure S6. Quantitative co-localization study of WIPI-1 and over-expressed GFP-2xFYVE. Using G361 cells transiently expressing GFP-2xFYVE, endogenous EEA1 or endogenous WIPI-1 was detected by indirect immunofluorescence. In addition, G361 cells transiently expressing both *myc*-tagged WIPI-1 and GFP-2xFYVE were subjected to anti-*myc* immunofluorescence. By confocal microscopy co-localization events (see arrows) were counted using 10 individual cells each. Endogenous as well as *myc*-tagged WIPI-1 co-localized with GFP-2xFYVE in 1 out of 10 cells (1 structure / cell). Bar: 20 μM.

Abbreviations

AMPK: AMP-activated protein kinase; Atg: Autophagy related; DMEM: Dulbecco's modified eagle medium; EBSS: Earl's balanced salt solution; FIP200: Focal adhesion kinase family kinase interacting protein of 200 kDa; FYVE: Fab1p YOTB, Vac1p, EEA1; LC3: Microtubule-associated protein light chain 3; mTOR: Mammalian target of rapamycin; mTORC1: Mammalian target of rapamycin complex 1; PIKfyve: FYVE finger-containing phosphoinositide kinase; PtdIns(3)P: Phosphatidylinositol 3-phosphate; PtdIns3KC3: Phosphatidylinositol 3-kinase class III; PtdIns(3,5)P_2: Phosphatidylinositol 3,5-bisphosphate; Ulk: UNC-51-like kinase; Vps: Vacuolar protein sorting; WIPI: WD-repeat protein interacting with phosphoinositides.

Competing interests

The authors declare they have no competing interests.

Authors' contributions

AG designed and conducted site-directed mutagenesis, characterized GFP-WIPI-1 mutants, analyzed the data and drafted the manuscript. DB carried out automated GFP-WIPI-1 puncta-formation analysis upon mTOR down regulation and analyzed the data. AH characterized the effect of YM201636 on WIPI-1 puncta formation and analyzed the data. TP-C conceived and designed the study, analyzed the data and wrote the manuscript. All authors read and approved the final manuscript.

Acknowledgements

We kindly acknowledge the phylogenetic analysis of the WIPI-1 propeller blades by Andrei Lupas, Max Planck Institute for Developmental Biology, Tuebingen, Germany. We thank Kenneth W. Berendzen from the Cytometric Unit (ZMBP) at the Eberhard Karls University Tuebingen for fluorescence-assisted cell sorting, and Anke Jacob and Simon Pfisterer from the Proikas-Cezanne laboratory for experimental support. This work was financed by grants from the Federal Ministry for Education and Science (BMBF BioProfile), Germany; the Ministry of Science, Research and Arts Baden-Wuerttemberg (Landesstiftung), and the German Research Foundation (DFG, SFB 773) to TP-C.

Received: 14 August 2012 Accepted: 24 September 2012
Published: 22 October 2012

References

1. Mizushima N, Levine B, Cuervo AM, Klionsky DJ: **Autophagy fights disease through cellular self-digestion.** *Nature* 2008, **451:**1069–1075.
2. Yang Z, Klionsky DJ: **Eaten alive: a history of macroautophagy.** *Nat Cell Biol* 2010, **12:**814–822.
3. Moreau K, Luo S, Rubinsztein DC: **Cytoprotective roles for autophagy.** *Curr Opin Cell Biol* 2010, **22:**206–211.
4. Singh R, Cuervo AM: **Autophagy in the cellular energetic balance.** *Cell Metab* 2011, **13:**495–504.
5. Hamasaki M, Yoshimori T: **Where do they come from? Insights into autophagosome formation.** *FEBS Lett* 2010, **584:**1296–1301.
6. Hayashi-Nishino M, Fujita N, Noda T, Yamaguchi A, Yoshimori T, Yamamoto A: **A subdomain of the endoplasmic reticulum forms a cradle for autophagosome formation.** *Nat Cell Biol* 2009, **11:**1433–1437.
7. Yla-Anttila P, Vihinen H, Jokitalo E, Eskelinen EL: **3D tomography reveals connections between the phagophore and endoplasmic reticulum.** *Autophagy* 2009, **5:**1180–1185.
8. Ravikumar B, Moreau K, Jahreiss L, Puri C, Rubinsztein DC: **Plasma membrane contributes to the formation of pre-autophagosomal structures.** *Nat Cell Biol* 2010, **12:**747–757.
9. Mari M, Griffith J, Rieter E, Krishnappa L, Klionsky DJ, Reggiori F: **An Atg9-containing compartment that functions in the early steps of autophagosome biogenesis.** *J Cell Biol* 2010, **190:**1005–1022.
10. Mizushima N, Yoshimori T, Ohsumi Y: **The role of Atg proteins in autophagosome formation.** *Annu Rev Cell Dev Biol* 2011, **27:**107–132.
11. Hosokawa N, Hara T, Kaizuka T, Kishi C, Takamura A, Miura Y, Iemura S, Natsume T, Takehana K, Yamada N, Guan JL, Oshiro N, Mizushima N: **Nutrient-dependent mTORC1 association with the ULK1-Atg13-FIP200 complex required for autophagy.** *Mol Biol Cell* 2009, **20:**1981–1991.
12. Jung CH, Jun CB, Ro SH, Kim YM, Otto NM, Cao J, Kundu M, Kim DH: **ULK-Atg13-FIP200 complexes mediate mTOR signaling to the autophagy machinery.** *Mol Biol Cell* 2009, **20:**1992–2003.
13. Egan DF, Shackelford DB, Mihaylova MM, Gelino S, Kohnz RA, Mair W, Vasquez DS, Joshi A, Gwinn DM, Taylor R, Asara JM, Fitzpatrick J, Dillin A, Viollet B, Kundu M, Hansen M, Shaw RJ: **Phosphorylation of ULK1 (hATG1) by AMP-activated protein kinase connects energy sensing to mitophagy.** *Science* 2011, **331:**456–461.
14. Lee JW, Park S, Takahashi Y, Wang HG: **The association of AMPK with ULK1 regulates autophagy.** *PLoS One* 2010, **5:**e15394.
15. Kim J, Kundu M, Viollet B, Guan KL: **AMPK and mTOR regulate autophagy through direct phosphorylation of Ulk1.** *Nat Cell Biol* 2011, **13:**132–141.
16. Blommaart EF, Luiken JJ, Blommaart PJ, van Woerkom GM, Meijer AJ: **Phosphorylation of ribosomal protein S6 is inhibitory for autophagy in isolated rat hepatocytes.** *J Biol Chem* 1995, **270:**2320–2326.
17. Petiot A, Ogier-Denis E, Blommaart EF, Meijer AJ, Codogno P: **Distinct classes of phosphatidylinositol 3'-kinases are involved in signaling pathways that control macroautophagy in HT-29 cells.** *J Biol Chem* 2000, **275:**992–998.
18. Knaevelsrud H, Simonsen A: **Lipids in autophagy: constituents, signaling molecules and cargo with relevance to disease.** *Biochim Biophys Acta* 2012, **1821:**1133–1145.
19. Obara K, Ohsumi Y: **PtdIns 3-Kinase Orchestrates Autophagosome Formation in Yeast.** *J Lipids* 2011, **2011:**498768.
20. Blommaart EF, Krause U, Schellens JP, Vreeling-Sindelarova H, Meijer AJ: **The phosphatidylinositol 3-kinase inhibitors wortmannin and LY294002 inhibit autophagy in isolated rat hepatocytes.** *Eur J Biochem* 1997, **243:**240–246.
21. Noda T, Matsunaga K, Taguchi-Atarashi N, Yoshimori T: **Regulation of membrane biogenesis in autophagy via PI3P dynamics.** *Semin Cell Dev Biol* 2010, **21:**671–676.
22. Noda T, Matsunaga K, Yoshimori T: **Atg14L recruits PtdIns 3-kinase to the ER for autophagosome formation.** *Autophagy* 2011, **7:**438–439.
23. Axe EL, Walker SA, Manifava M, Chandra P, Roderick HL, Habermann A, Griffiths G, Ktistakis NT: **Autophagosome formation from membrane compartments enriched in phosphatidylinositol 3-phosphate and dynamically connected to the endoplasmic reticulum.** *J Cell Biol* 2008, **182:**685–701.
24. Polson HE, de Lartigue J, Rigden DJ, Reedijk M, Urbe S, Clague MJ, Tooze SA: **Mammalian Atg18 (WIPI2) localizes to omegasome-anchored phagophores and positively regulates LC3 lipidation.** *Autophagy* 2010, **6:**506–522.
25. Itakura E, Mizushima N: **Characterization of autophagosome formation site by a hierarchical analysis of mammalian Atg proteins.** *Autophagy* 2010, **6:**764–776.
26. Simonsen A, Birkeland HC, Gillooly DJ, Mizushima N, Kuma A, Yoshimori T, Slagsvold T, Brech A, Stenmark H: **Alfy, a novel FYVE-domain-containing protein associated with protein granules and autophagic membranes.** *J Cell Sci* 2004, **117:**4239–4251.
27. Ridley SH, Ktistakis N, Davidson K, Anderson KE, Manifava M, Ellson CD, Lipp P, Bootman M, Coadwell J, Nazarian A, Erdjument-Bromage H, Tempst P, Cooper MA, Thuring JW, Lim ZY, Holmes AB, Stephens LR, Hawkins PT: **FENS-1 and DFCP1 are FYVE domain-containing proteins with distinct functions in the endosomal and Golgi compartments.** *J Cell Sci* 2001, **114:**3991–4000.
28. Isakson P, Holland P, Simonsen A: **The role of ALFY in selective autophagy.** *Cell Death Differ* 2012, doi:doi: 10.1038/cdd.2012.66. [Epub ahead of print].
29. Proikas-Cezanne T, Waddell S, Gaugel A, Frickey T, Lupas A, Nordheim A: **WIPI-1alpha (WIPI49), a member of the novel 7-bladed WIPI protein family, is aberrantly expressed in human cancer and is linked to starvation-induced autophagy.** *Oncogene* 2004, **23:**9314–9325.
30. Krick R, Busse RA, Scacioc A, Stephan M, Janshoff A, Thumm M, Kühnel K: **Structural and functional characterization of the two phosphoinositide binding sites of PROPPINs, a beta-propeller protein family.** *Proc Natl Acad Sci USA* 2012, **109:**E2042–E2049.
31. Baskaran S, Ragusa MJ, Boura E, Hurley JH: **Two-Site Recognition of Phosphatidylinositol 3-Phosphate by PROPPINs in Autophagy.** *Mol Cell* 2012, **3:**339–348.
32. Mauthe M, Jacob A, Freiberger S, Hentschel K, Stierhof YD, Codogno C, Proikas-Cezanne T: **Resveratrol-mediated autophagy requires WIPI-1-regulated LC3 lipidation in the absence of induced phagophore formation.** *Autophagy* 2011, **7:**1448–1461.
33. Proikas-Cezanne T, Robenek H: **Freeze-fracture replica immunolabelling reveals human WIPI-1 and WIPI-2 as membrane proteins of autophagosomes.** *J Cell Mol Med* 2011, **15:**2007–2010.
34. Tooze SA, Jefferies HB, Kalie E, Longatti A, McAlpine FE, McKnight NC, Orsi A, Polson HE, Razi M, Robinson DJ, Webber JL: **Trafficking and signaling in mammalian autophagy.** *IUBMB Life* 2010, **62:**503–508.
35. Codogno P, Mehrpour M, Proikas-Cezanne T: **Canonical and non-canonical autophagy: variations on a common theme of self-eating?** *Nat Rev Mol Cell Biol* 2012, **13:**7–12.
36. Jeffries TR, Dove SK, Michell RH, Parker PJ: **PtdIns-specific MPR pathway association of a novel WD40 repeat protein, WIPI49.** *Mol Biol Cell* 2004, **15:**2652–2663.
37. Proikas-Cezanne T, Ruckerbauer S, Stierhof YD, Berg C, Nordheim A: **Human WIPI-1 puncta-formation: a novel assay to assess mammalian autophagy.** *FEBS Lett* 2007, **581:**3396–3404.
38. Proikas-Cezanne T, Pfisterer SG: **Assessing mammalian autophagy by WIPI-1/Atg18 puncta formation.** *Methods Enzymol* 2009, **452:**247–260.
39. Mauthe M, Yu W, Krut O, Krönke M, Gotz F, Robenek H, Proikas-Cezanne T: **WIPI-1 Positive Autophagosome-Like Vesicles Entrap Pathogenic Staphylococcus aureus for Lysosomal Degradation.** *Int J Cell Biol* 2012, **2012:**179207.
40. Jefferies HB, Cooke FT, Jat P, Boucheron C, Koizumi T, Hayakawa M, Kaizawa H, Ohishi T, Workman P, Waterfield MD, Parker PJ: **A selective PIKfyve inhibitor blocks PtdIns(3,5)P(2) production and disrupts endomembrane transport and retroviral budding.** *EMBO Rep* 2008, **9:**164–170.
41. Pfisterer SG, Mauthe M, Codogno P, Proikas-Cezanne T: **Ca2+/calmodulin-dependent kinase (CaMK) signaling via CaMKI and AMP-activated protein kinase contributes to the regulation of WIPI-1 at the onset of autophagy.** *Mol Pharmacol* 2011, **80:**1066–1075.
42. Berendzen KW, Bohmer M, Wallmeroth N, Peter S, Vesi M, Zhou Y, Tiesler FK, Schleifenbaum F, Harter K: **Screening for in planta protein-protein interactions combining bimolecular fluorescence complementation with flow cytometry.** *Plant Methods* 2012, **8:**25.

43. Frickey T, Lupas A: **CLANS: a Java application for visualizing protein families based on pairwise similarity.** *Bioinformatics* 2004, **20:**3702–3704.
44. Van de Peer Y, Frickey T, Taylor J, Meyer A: **Dealing with saturation at the amino acid level: a case study based on anciently duplicated zebrafish genes.** *Gene* 2002, **295:**205–211.

doi:10.1186/1750-2187-7-16
Cite this article as: Gaugel *et al.*: Defining regulatory and phosphoinositide-binding sites in the human WIPI-1 β-propeller responsible for autophagosomal membrane localization downstream of mTORC1 inhibition. *Journal of Molecular Signaling* 2012 **7**:16.